

13. G. Bertotti, *Hysteresis in Magnetism* (Academic Press, New York, 1998).
14. A. P. Malozemoff and J. C. Slonczewski, *Magnetic Domain Wall in Bubble Materials* (Academic Press, New York, 1979).
15. Kirilyuk *et al.*, *J. Magn. Magn. Mater.* **171**, 45 (1997).
16. We thank Y. Otani and R. Haßdorf for valuable discussions and N. Osada for experimental assistance. Supported by a grant-in-aid for scientific research on priority area from Monbusho in Japan.

15 December 1998; accepted 23 February 1999

Magnetization Directions of Individual Nanoparticles

S. A. Majetich* and Y. Jin

The magnetization directions of individual monodomain nanoparticles as small as 5 nanometers in diameter are determined using the Foucault method of Lorentz microscopy. A model is developed to explain the images and diffraction patterns of samarium cobalt nanoparticles as a function of the aperture shift direction. Thermally induced changes in the magnetization direction of superparamagnetic magnetite nanoparticles were observed but with a much slower rate than expected, due to surface anisotropy. When the time scale for magnetization reversal is much shorter than the data acquisition time, as in carbon-coated iron cobalt alloy nanoparticles, the images show an average of such thermally induced changes.

The ability to determine the magnetization direction of a monodomain nanoparticle is of great interest, particularly as the bit density of magnetic recording media is increased. In particulate media, a threshold is reached when the size of the particles or uncoupled grains approaches the superparamagnetic limit (1), which is ~ 10 nm for Co. Below this size, thermal fluctuations are sufficient to change the magnetization direction, and the ability to store information is lost. The maximum size for superparamagnetic behavior, below which the magnetization reversal field or coercivity H_c drops to zero, and the maximum monodomain size, where H_c is maximized, can be estimated for different materials (2–4). However, the predictions fail for compounds with either very high or very low magnetocrystalline anisotropy (5, 6). The Stoner-Wohlfarth theory (7) predicts the size-dependent coercivity for isolated ellipsoidal monodomain particles, but the experimental H_c is always lower, a result known as Brown's Paradox (8).

We report the extension of Lorentz microscopy to determine the magnetization direction in SmCo_5 , Fe_3O_4 , and carbon-coated $\text{Fe}_{50}\text{Co}_{50}$ nanoparticles as small as 5 nm. Although micro-SQUIDS (superconducting quantum interference devices) (9, 10) enable the magnetization M to be determined quantitatively, it is difficult to study a large number of different particles individually. Alternatively, magnetization directions can be determined by Lorentz microscopy and magnetic force microscopy (MFM). In order to

realize the quantum disk (11), where each particle is an individual bit, a nondestructive method such as MFM would be required. However, for features smaller than 100 nm, Lorentz microscopy is currently superior (12), and this technique was therefore used in this study.

Two types of Lorentz microscopy have previously been used to study small particles, the Fresnel and Foucault methods. In the Fresnel method (13), the sample is imaged with the plane of focus above or below the specimen. Where M of the sample is changing, such as in the domain walls of a thin film, electron trajectories either converge or diverge and appear as bright or dark regions in the image, respectively. Hütten *et al.* (14) investigated Co precipitates with particle diameters of 50 to 100 nm in $\text{Au}_{72}\text{Co}_{28}$ alloy thin films and compared the images with simulations based on electron trajectories. The spherical particles appeared either entirely bright or entirely dark and reversed their contrast between underfocus and overfocus conditions. The particles were first modeled as single domains, with a varying magnetization direction with respect to the vertical axis. These simulations predicted asymmetric images, in contrast to the actual observations. A modified model assumed magnetization reversal by curling, with no external fringe field. Contrast dependent only on the curling direction of the particle magnetic induction relative to the incident electron velocities was used to explain the experimental observations of bright and dark spots at the locations of the Co particles.

Foucault method Lorentz microscopy was done by Salling *et al.* (15) on needle-shaped $\gamma\text{-Fe}_2\text{O}_3$ particles on the order of 65 nm in

diameter and 300 nm in length. In the Foucault method (16), the objective aperture is shifted to block electrons that have passed through parts of the sample magnetized in a particular direction, causing these regions to appear dark in the resulting image. This aperture is located in the back focal plane of the objective lens, where the electron intensity is in the form of the diffraction pattern for the sample. For a thin film containing two domains with opposite M values, shifting the aperture can make one entire domain dark and the other bright, or vice versa, depending on the direction of the shift. The fine particles of $\gamma\text{-Fe}_2\text{O}_3$ were magnetized along the long axis, and when the aperture was shifted, dark lobes appeared on both sides of the particle, which were attributed to the fringe field. When the same particle was magnetized in the opposite direction, no dark lobes were visible, and the particle appeared the same as in the bright-field image.

We extend the size range to even smaller particles, some of which are below the superparamagnetic limit, and present a model for interpreting the images. First, the Foucault Lorentz microscopy method was used to image nanoparticles of the high anisotropy alloy SmCo_5 , revealing features not observed in the larger, elongated particles studied by Salling *et al.* (15). Details of the preparation of these ball-milled nanoparticles have been reported elsewhere (17). In this material, the superparamagnetic limit is 2 nm, and larger particles are expected to have stable magnetization directions. The results as a function of the aperture shift direction provide the basis for interpreting the Lorentz microscopy images of extremely small particles. Next, this method was applied to two systems expected to contain superparamagnetic particles: Fe_3O_4 nanoparticles from a ferrofluid (18) (EMG-705; Ferrofluidics Corp., Nashua, New Hampshire) and carbon-coated $\text{Fe}_{50}\text{Co}_{50}$ nanoparticles made in a plasma torch (19). Although magnetization reversal occurs on a nanosecond time scale and the dynamics are not observed directly, particles may exist in metastable states for minutes or even hours between thermal switching events (20).

Foucault Lorentz microscopy was carried out in a JEM-120CX (JEOL, Sundbyberg, Sweden) transmission electron microscope (TEM) with a Lorentz pole piece, so that the sample was loaded into a magnetic field-free region. Lorentz microscopy was also performed using a JEOL 4000 EX electron microscope equipped with a Gatan imaging energy filter and used with an objective minilens in order to keep the sample in a field-free region. The particles were examined under bright-field conditions, and then the objective aperture was shifted to cut off part of the electron beam transmitted by the sample. Images of SmCo_5 nanoparticles were recorded for a series of different aperture shift direc-

Department of Physics, Carnegie Mellon University, Pittsburgh, PA 15213-3890, USA.

*To whom correspondence should be addressed. E-mail: sm70@andrew.cmu.edu

REPORTS

tions, and a diffraction pattern was also taken for each aperture shift. The aperture shift angles θ_A were found from the diffraction patterns and corrected for rotation.

Bright-field images show spherical SmCo_5 particles 5 to 50 nm in diameter that were well dispersed in a thermoplastic matrix (Fig. 1A). With all aperture shifts, a pair of dark lobes separated by 180° appeared on either side of each particle. The orientation of the lobes was the same for all of the particles, and the size of the lobes scaled with the particle diameter. As the aperture shift angle θ_A was increased, the dark lobes at angles θ_{\min} tilted (Fig. 1, B through F). Figure 2 summarizes the relation between θ_{\min} and θ_A . At some aperture shift angles, the center of the particles became dark and was surrounded by a bright ring as well as the pair of dark lobes (Fig. 1B). Increasing the magnitude of the shift for a given direction increased the size of the dark centers and made dark centers appear in smaller particles. The diffraction patterns associated with these images (Fig. 3) showed a diffuse spot with a faint sharp spike through the center and were offset according to the aperture shift direction.

The dark lobes are evidence of the fringe field of the magnetic particle, whereas the angle at which the dark center is maximized reveals its magnetization direction. From the Abbe theory of image formation, the back focal plane of a lens contains the Fourier transform of the object transform (21). The magnetic nanoparticle can be treated as a phase object with a spatially varying Aharonov-Bohm phase shift (22) induced in the wave function of electrons passing through different regions. The difference in phase between two electron trajectories along vectors \mathbf{r}_1 and \mathbf{r}_2 is given by (23)

$$\Delta\phi(r_1, r_2) = \frac{2\pi e}{h} \int_{-\infty}^{\infty} dy \int_{r_1}^{r_2} \mathbf{B}(x, y, z) \cdot [\hat{e}_y \times d(\mathbf{r}_2 - \mathbf{r}_1)] \quad (1)$$

where the electrons are initially traveling in the y direction, and \mathbf{B} is the magnetic induction that causes Lorentz deflection. When the phase shifts are small for electrons passing through or close to a nanoparticle, the wave function can be expanded (24)

$$\psi(r) \sim e^{i\phi(r)} \approx 1 - i\phi(r) \quad (2)$$

For a thin horizontal slice of the samples, the inhomogeneous part of the wave function is proportional to the horizontal component of \mathbf{B} . A monodomain particle modeled as a uniformly magnetized sphere has magnetic induction (25) inside

$$\mathbf{B} = \frac{8\pi}{3} M_0 \hat{e}_z \quad (3a)$$

and outside in the fringe field,

$$\mathbf{B} = \frac{4\pi}{3} M_0 a^3 \times \left[\frac{3xz}{r^5} \hat{e}_x + \frac{3yz}{r^5} \hat{e}_y + \frac{(3z^2 - r^2)}{r^5} \hat{e}_z \right] \quad (3b)$$

where M_0 is the magnetization and a is the radius.

We first consider the fringe field components. Although the fringe field of the particle does not affect the amplitude of the electron wave function, its phase is shifted and the electron direction is altered. For each point at a fixed distance outside the particle at an angle θ , there is a corresponding point at $\theta + \pi$ with the same value of \mathbf{B} , just as for a point dipole. When the aperture shift blocks electrons deflected in a given direction by the fringe field, two minima separated by 180°

are observed (Fig. 1; the pair of dark lobes). Because the back focal plane contains the Fourier transform of the object wave function, the spatial distribution of electron intensity is altered. Just as in Young's single-slit diffraction experiment, dimensions that are large in the object are small in its Fourier transform, and vice versa. In the fringe field of the particle, lines of constant \mathbf{B} turn inward at the ends ($\theta = 0^\circ, 180^\circ$) relative to the magnetization direction. In the diffraction pattern, there are small spike-like outward extensions at 90° and 270° , as seen experimentally (Fig. 3). Shifting the aperture at an angle θ_A in the back focal plane blocks electrons that have passed through the sample perpendicular to this angle, so that dark lobes appear in the image at angles $\theta_{\min} = \theta_A \pm \pi/2$, in agreement with the data of Fig. 2.

The appearance of the dark center with intensity maximized for a unique value of θ_M can be explained from the Lorentz deflection of electrons passing through the uniformly magnetized particle interior. All electrons are deflected in the same direction while passing through the particle, but those passing through the center are most deflected. This condition creates a unique aperture shift angle θ_{A^*} to reverse contrast in the particle interior and causes the center of the particle

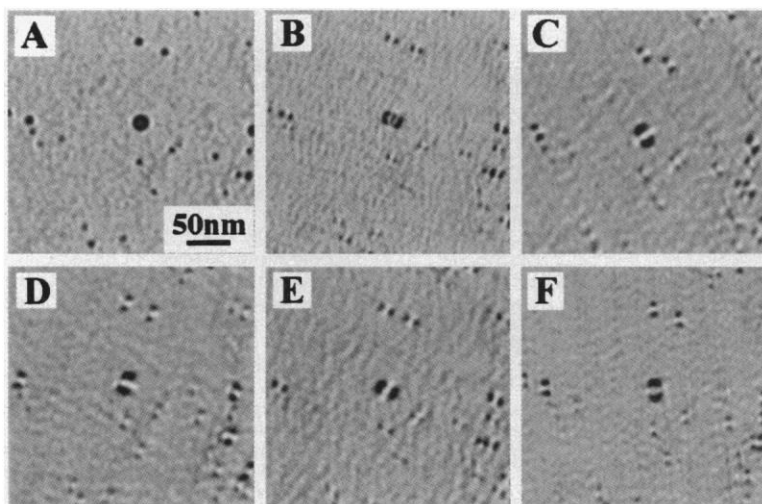


Fig. 1. (A) Bright-field image of a SmCo_5 nanoparticle. Foucault Lorentz images are shown for different aperture shift angles, θ_A : (B) 55° , (C) 81° , (D) 145° , (E) 207° , and (F) 252° .

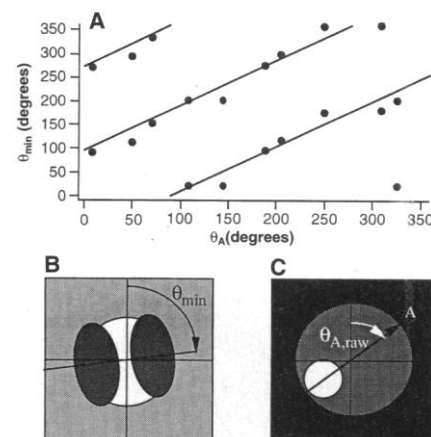


Fig. 2. (A) Plot of the dark lobe angles, θ_{\min} , versus the aperture shift angle, θ_A . Points indicate experimental values, while the lines illustrate the least squares fit to the data. The fit yields minima at $\theta_{\min} = 0.951 \theta_A + 94.7^\circ$ and $\theta_{\min} = 0.951 \theta_A + 184.7^\circ$. To determine θ_{\min} and $\theta_{A, \text{raw}}$ the Lorentz image and associated diffraction pattern for a given aperture shift were compared. Using the same coordinate system, θ_{\min} was found from the bisector of the dark lobes (B), while $\theta_{A, \text{raw}}$ was obtained from the shift of the diffraction pattern (white spot) from the center of the field of view (C). The vector \mathbf{A} indicates the aperture shift direction. There is an associated rotation between diffraction-mode and bright field-mode images for each microscope, which was 40° counterclockwise for the JEM 120CX. The θ_A value was obtained by correcting the raw data for this rotation.

REPORTS

to darken first. After accounting for image inversion in the lens, the true orientation of the particle magnetic moment, θ_M , is given by

$$\theta_M = \theta_A + \pi/2 \quad (4)$$

Unlike the results from Salling *et al.* (15), in the small SmCo_5 particles, the phase shift dominates the amplitude effect and the centers of the particles become bright in the Foucault Lorentz imaging, except when $\theta_M = \theta_A^* + \pi/2$. The new results show that the appearance of dark lobes does not specify the magnetic moment direction for small spherical particles, although this feature is more prominent than the particle interior. In small but ellipsoidal SmCo_5 nanoparticles with aspect ratios of approximately 3:1, elongated dark lobes were observed, and for a unique direction of the aperture shift, the contrast roughly reversed, so that the interior of the particle appeared dark with a pair of bright lobes on either side. The ability to see contrast reversal here but not in the spheres is due to the larger size of the elongated particles, rather than their shape. Unlike the results of Hütten *et al.* (14), the data for the SmCo_5 nanoparticles show the presence of fringe fields, and there is no evidence that the particle magnetization is nonuniform, as required by the curling model. However, the SmCo_5 nanoparticles are well within the monodomain limit, whereas the Co nanoparticles in Au were at or slightly above the threshold for monodomain behavior.

The Lorentz microscopy technique and image interpretation model were next applied to nanoparticles expected to exhibit superparamagnetic behavior. In a superparamagnet, the rate of thermally induced switching is given by

$$\tau^{-1} = \tau_o^{-1} \exp(-KV/kT) \quad (5)$$

where τ_o^{-1} is approximately equal to the Larmor precession frequency, K is the magnetocrystalline anisotropy, V is the particle volume, k is Boltzmann's constant, and T is temperature. Because the rate is so strongly dependent on the particle diameter, small changes in size may greatly affect the stability of the magnetization direction.

In a 10-nm Fe_3O_4 nanoparticle, the average switching time τ was calculated to be ~ 5 ns. Two images are shown of a particle taken 10 min apart (Fig. 4), in which the aperture shift angle θ_A required to darken the particle center changes. This result indicates that the magnetization direction changes, but on a time scale much slower than the 5 ns predicted from Eq. 5 and the bulk value of $K = 1.2 \times 10^5$ ergs/cm³ (26). However, extremely high coercivity has previously been observed in NiFe_2O_4 nanoparticles (27), which at 4.2 K had some particles reversing their magnetization directions at fields up to 40 times the anisotropy field $H_K = 2K/M_s$. This result was attributed to a spin-glass-like layer or disordered spins on the particle surface. The effective anisotropy of the individual Fe_3O_4 nanoparticles we observed must be 20 to 25 times the value of the bulk magnetocrystalline anisotropy, based on the magnitude of the time between thermally induced switching events.

Where magnetization changes were seen in these Fe_3O_4 nanoparticles, the rotation angle was either 90° or 180° . The $\langle 111 \rangle$ directions are easy axes for magnetization in

Fe_3O_4 (28). If the crystal is oriented with the $\langle 100 \rangle$ crystallographic direction parallel to the electron beam direction, the projections of the easy axes onto the plane would be 90° or 180° , relative to each other. Particles with this orientation may have been noted preferentially because of the strong in-plane component of the magnetization, both before and after it changed direction.

In the 10-nm $\text{Fe}_{50}\text{Co}_{50}$ nanoparticles, where the average switching time $\tau \approx 2$ ns based on the bulk magnetocrystalline anisotropy (29), the images were consistent with an average of those for different magnetization orientations, as expected for a superparamagnet. These particles showed slightly darkened centers at all aperture shift angles θ_A . The contrast in the interior of the particles was less than that for SmCo_5 or Fe_3O_4 and more rounded. In particles with stable magnetization directions during the data acquisition time, the dark centers were elongated in the magnetization direction. Along this axis, the phase shift in the fringe field above and below the particle adds to that for the particle interior; perpendicular to this axis, the phase shifts partially cancel.

The Foucault method of Lorentz microscopy has potential for application to a number of interesting problems in nanoscale magnetism. Size-dependent magnetization reversal fields could be differentiated from the effects of grain boundaries, surface roughness, and oxide shells. It could be used to determine the superparamagnetic threshold and maximum monodomain sizes in low-anisotropy alloys like $\text{Fe}_{50}\text{Co}_{50}$, where factors such as magnetostriction may affect the overall anisotropy. Finally, it could be applied to interacting systems, as in magnetic data storage media, to see if neighboring particles or grains were coupled by exchange or dipolar interactions, and to determine their optimal separation for maximum coercivity and individually addressable bits.

References and Notes

1. S. H. Charap, P. L. Lu, Y. He, *IEEE Trans. Magn.* **33**, 978 (1997).
2. E. F. Kneller and F. E. Luborsky, *J. Appl. Phys.* **34**, 656 (1963).
3. E. Kneller, in *Magnetism and Metallurgy*, A. Berkowitz and E. Kneller, Eds. (Academic Press, New York, 1969), p. 385.
4. B. D. Cullity, *Introduction to Magnetic Materials* (Addison-Wesley, Reading, MA, 1972), p. 301.
5. For a soft magnetic material such as $\text{Fe}_{50}\text{Co}_{50}$, the superparamagnetic limit, 34 nm, is predicted to be greater than the maximum monodomain size, 8.5 nm.
6. R. A. McCurrie and G. P. Carswell, *J. Mater. Sci.* **5**, 825 (1970).
7. E. C. Stoner and E. P. Wohlfarth, *Philos. Trans. R. Soc. London Ser. A* **240**, 599 (1948).
8. W. F. Brown Jr., *J. Appl. Phys.* **29**, 470 (1958); K. D. Durst and H. Kronmüller, *J. Magn. Magn. Mater.* **68**, 63 (1987).
9. W. Wernsdorfer *et al.*, *Phys. Rev. Lett.* **78**, 1791 (1997).
10. A. D. Kent, T. M. Shaw, S. von Molnár, D. D.



Fig. 3. Diffraction pattern associated with the images of Fig. 1B. The arrow indicates the aperture shift direction, uncorrected for the rotation of the image relative to the diffraction pattern. Note the spike passing through the central spot. When the aperture shift direction is normal to this spike, a dark center appears in the image of the particle.

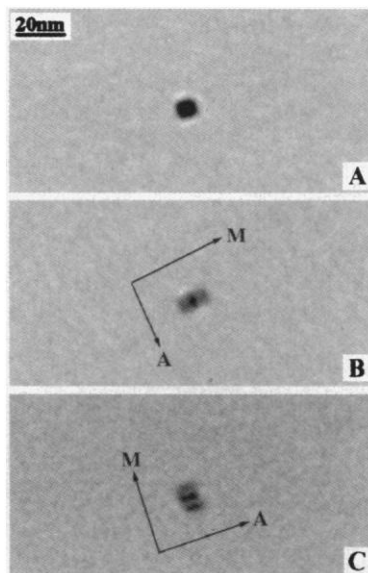


Fig. 4. (A) Bright-field image of a Fe_3O_4 nanoparticle; (B and C) Lorentz images of the particle for different aperture shift directions A , which yield a dark center and therefore magnetization direction M . Note that the magnetization direction of this particle has changed between (B) and (C).

- Awschalom, *Science* **262**, 1249 (1993); J. Shi, S. Gider, K. Babcock, D. D. Awschalom, *ibid.* **271**, 937 (1996).
11. S. Y. Chou, P. R. Krauss, L. Kong, *J. Appl. Phys.* **79**, 6101 (1996).
 12. J. Dooley and M. De Graef, *Ultramicroscopy* **67**, 113 (1997); M. De Graef, N. T. Nuhfer, M. R. McCartney, *J. Microsc.*, in press.
 13. H. W. Fuller and M. E. Hale, *J. Microsc.* **31**, 238 (1960).
 14. A. Hütten, J. Bernardi, C. Nelson, G. Thomas, *Phys. Status Solidi A* **150**, 171 (1995).
 15. C. Salling, S. Schultz, I. McFayden, M. Ozaki, *IEEE Trans. Magn.* **27**, 5184 (1991); G. A. Gibson, J. F. Smyth, S. Schultz, D. P. Kern, *ibid.*, p. 5187; M. Lederman, G. A. Gibson, S. Schultz, *J. Appl. Phys.* **73**, 6961 (1993).
 16. H. W. Fuller and M. E. Hale, *J. Appl. Phys.* **31**, 1699 (1960).
 17. S. A. Majetich and E. M. Kirkpatrick, *IEEE Trans. Magn.* **33**, 3721 (1997); S. A. Majetich *et al.*, *Nanostruct. Mater.* **9**, 291 (1997).
 18. Based on the size criterion for superparamagnetic behavior given in (2), 10-nm particles of Fe₃O₄ are expected to be superparamagnetic at room temperature. As found experimentally in J. Zhang, C. Boyd, and W. Luo [*Phys. Rev. Lett.* **77**, 390 (1996)], when a ferrofluid is diluted so that the particle separation is large (as in the TEM samples we studied), Néel relaxation or superparamagnetic behavior is observed.
 19. J. H. Scott and S. A. Majetich, *Phys. Rev. B* **52**, 12564 (1995); Z. Turgut, J. H. Scott, M. Q. Huang, S. A. Majetich, M. E. McHenry, *J. Appl. Phys.* **83**, 6468 (1998).
 20. B. D. Cullity, *Introduction to Magnetic Materials* (Addison-Wesley, Reading, MA, 1972), p. 413.
 21. M. Born and E. Wolf, *Principles of Optics* (Pergamon, Oxford, 1970), p. 420.
 22. Y. Aharonov and D. Bohm, *Phys. Rev.* **115**, 485 (1959).
 23. D. Wohlleben, *J. Appl. Phys.* **38**, 3341 (1967).
 24. Z. L. Wang, *Adv. Mater.* **10**, 13 (1998).
 25. J. D. Jackson, *Classical Electrodynamics* (Wiley, New York, 1975), pp. 178 and 196–197.
 26. R. A. McCurrie, *Ferromagnetic Materials: Structure and Properties* (Academic Press, New York, 1994), p. 142.
 27. R. H. Kodama, A. E. Berkowitz, E. J. McNiff Jr., S. Foner, *Phys. Rev. Lett.* **77**, 394 (1996).
 28. C. W. Chen, *Magnetism and Metallurgy of Soft Magnetic Materials* (Dover, New York, 1986), p. 211.
 29. F. Pfeifer and C. Radeloff, *J. Magn. Magn. Mater.* **19**, 190 (1980).
 30. We thank J. Suhan for microtomy sectioning and J. H. Scott for helpful discussions. S.A.M. thank NSF for financial support (awards DMR-9285308 and DMR-9500313).

16 December 1998; accepted 17 February 1999

A Steric Mechanism for Inhibition of CO Binding to Heme Proteins

Galina S. Kachalova, Alexander N. Popov,* Hans D. Bartunik†

The crystal structures of myoglobin in the deoxy- and carbon monoxide-ligated states at a resolution of 1.15 angstroms show that carbon monoxide binding at ambient temperatures requires concerted motions of the heme, the iron, and helices E and F for relief of steric inhibition. These steps constitute the main mechanism by which heme proteins lower the affinity of the heme group for the toxic ligand carbon monoxide.

The structural basis of the discrimination between O₂ and the toxic ligand CO by heme proteins has been the subject of many experimental and theoretical investigations (1). Aside from their role in respiration, CO ligands may act as regulators of cell and organ function (2). In addition to environmental sources, CO is produced endogenously in the breakdown of heme. The binding affinity of CO to heme proteins is much lower in comparison to that of porphyrin complexes. The textbook explanation of this difference is centered on the Fe-C-O binding geometry. Whereas this geometry is approximately linear in CO porphyrin complexes (3, 4), previously reported x-ray and neutron crystal structures of CO-ligated myoglobin (MbCO) show bent binding geometries with substantial deviations from linearity (5). In attempts to interpret these structural data and many infrared (IR) measurements, a number of models have been suggested in which bending of the Fe-CO unit is explained in terms of

short-range interactions between the ligand and the distal His of the protein matrix. It was proposed that steric repulsion (6), electrostatic interactions between the distal His side chain and the ligand involving strong back-bonding in the Fe-CO unit (7, 8), or a non-equilibrium orientation of the proximal His (9) may prevent the CO from binding in a linear conformation. However, recent results from IR polarization (10–12), Fourier transform IR spectroscopy (13), and a joint analysis of nuclear magnetic resonance, Fe⁵⁷ Mössbauer, and IR spectroscopic data (14) suggested a nearly linear geometry as the most likely conformation. These results and the large variability in the three-dimensional (3D) structural models raised severe doubts as to the accuracy of the previous crystal structure analyses.

We report the results of x-ray crystallographic studies of native sperm-whale myoglobin at ultrahigh resolution. Essentially unrestrained refinement (Table 1) at a resolution of 1.15 Å of the P₂₁ crystal structures of deoxy myoglobin (deoxyMb), MbCO, and aquo-met myoglobin (metMb) at pH 6 provided a very high accuracy (average error of 0.03 Å in the positions of main-chain atoms). The structural models differ substantially from the previous crystal structures, in particular with respect to the ligand binding geometry and to the interac-

tions between the ligand and residues inside the distal pocket. Some of these structural differences can be explained by heterogeneities in the ligation states that were not identified in previous crystal structures because of the lower resolution. A comparison of our MbCO and deoxyMb structures provided the basis for analyzing the structural mechanism of CO inhibition. The diffraction studies have been undertaken at room temperature in order to approach physiological conditions as closely as possible.

The MbCO crystal structure shows the individual atoms of the bound CO with full occupancy in a well-resolved electron density (Fig. 1). The ligand adopts a single conformation. The Fe-C-O binding geometry is nearly linear (Fig. 1 and Table 2); the angular deviation θ of the Fe-CO unit from linearity is 7.4° (1.9°) (numbers in parentheses are standard errors of the last digit or digits). The Fe-C bond is tilted by an angle $\tau = 4.7^\circ$ (0.9°) with respect to the normal to the nitrogen plane that is formed by the four pyrrole N ligands that surround the heme Fe in a nearly perfect square planar symmetry. Our results confirm theoretical estimates by Ray *et al.* (8) and remove the controversy between spectroscopy and previous crystal structures, which were interpreted in terms of more strongly inclined binding geometries and disordered CO sites (5). The angular geometry of the Fe-CO unit in the crystal structure is in close agreement with recent spectroscopic data for MbCO in solution (10–12, 14) and in the P₂₁ and P₂₁2₁2₁ crystal forms (10–12). When comparing the structures of MbCO and unencumbered porphyrin complexes, we found that the deviation of the Fe-CO unit from linearity (Table 2) is slightly stronger, by a few degrees, in MbCO. This additional distortion involves energies that are too small to explain the reduced binding affinity of CO to Mb (10–12). The Fe-C and the C-O bond lengths agree within the experimental errors (Table 2).

The internal structure of the heme is rather insensitive to the binding of CO. The tilt angles between the individual pyrrole rings and the nitrogen plane are nearly the same in MbCO

Max-Planck-Arbeitsgruppen für Strukturelle Molekularbiologie, Arbeitsgruppe Proteindynamik, Notkestraße 85, 22603 Hamburg, Germany.

*Present address: European Molecular Biology Laboratory Outstation, Notkestraße 85, 22603 Hamburg, Germany.

†To whom correspondence should be addressed. E-mail: bartunik@mpghdb.desy.de